A Reduced-Size Silicon Micromachined High-Q Resonator at 5.7 GHz

Christophe A. Tavernier, Rashaunda M. Henderson, *Member, IEEE*, and John Papapolymerou, *Member, IEEE*

***Abstract*—This paper depicts the progress toward a novel high-quality-factor miniaturized resonator operating in the 5.6–5.8-GHz range. The design of the resonator is based on a micromachined cavity loaded with a high dielectric-constant material. Energy is coupled into the cavity from input and output microstrip lines via slots. Quality factors up to 640 are demonstrated on silicon planar structures with a volume of 177 mm^3. Further size reduction yields a volume of 24.5 mm^3 and quality factors ranging from 152 to 197, while keeping the resonator integration ability. Bonding techniques and the dielectric loss of the loading material are proven to be the limiting factors in achieving higher quality factors.**

***Index Terms*—High-Q resonators, micromachining, planar circuit, small size.**

I. Introduction

With the ever-increasing demand of broad-band and mobile wireless communication systems, the need for high-performance, low-cost, low-power, and small-size RF/microwave circuits becomes more pronounced. Recently, there has been a strong motivation for microwave components operating around 5–7 GHz due to the advent of wireless local area networks (WLANs) for computer interconnections, personal communication systems (PCSs) and the European High Performance Radio Local Area Network (HIPERLAN). One of the most important components in such a wireless system is the bandpass filter that is used both in the receiver and transmitter for keeping unwanted signals away from other parts of the system. In order to achieve the superior performance required by the broad-band wireless communication systems and also comply with usually strict frequency regulations, these filters need to be designed with high-quality-factor resonators.

High-quality-factor resonators are typically built with waveguide components. In the frequency range of 5–7 GHz, waveguides are very large, very difficult to integrate with other planar circuits, and costly to manufacture. As an alternative, several researchers have been studying surface acoustic wave (SAW) and bulk acoustic wave (BAW) resonators [1]–[4]. These resonators provide a high quality factor at frequencies around 200 MHz–1.5 GHz ($11000 > Q_u > 3000$), but their fabrication requires submicrometer technologies above 2.4 GHz ($Q_u \sim 1500$), thus limiting for the time being their mass production and increasing their cost. In parallel, resonators using high dielectric materials based on stripline and microstrip-line technology have been explored [5], [6]. These resonators operate at lower frequencies and also have a typically lower Q performance. During the last five years, several groups have developed silicon micromachined cavity and membrane resonators that can provide superior quality factors at microwave frequencies [7], [8]. A micromachined millimeter-wave dielectric resonator, based on whispering-gallery modes, has also been reported [9]. These resonators are planar, monolithic, and have a low production cost, but for frequencies around 6 GHz, are limited by their size.

This paper will present a novel reduced-size high-Q silicon micromachined resonator around 5.7 GHz. Reduction in size is achieved by filling a silicon micromachined cavity with a high dielectric-constant material, such as barium strontium titanate (BST-$\varepsilon_r = 70$) and alumina ($\varepsilon_r = 9.8$). The development of the silicon resonator was based on a Duroid cavity model that was initially investigated [10].

II. Theory and Design

The design of the micromachined loaded cavity resonators is based on the theory of rectangular cavities. The resonators are operated in the fundamental TE_{101} mode. The following equations can be used to evaluate various parameters of the rectangular resonator [11]:

$$f_{\mathrm{res}} = \frac{c}{2\sqrt{\varepsilon_r}}\sqrt{\left(\frac{m}{l}\right)^2 + \left(\frac{n}{h}\right)^2 + \left(\frac{o}{w}\right)^2} \tag{1}$$

$$Q_c = \frac{(klw)^3 h\eta}{2\pi^2 R_m\left(2w^3h + 2l^3h + w^3l + l^3w\right)} \tag{2}$$

where

$$\begin{aligned} R_m &= \frac{1}{\sigma\delta_s} = \sqrt{\frac{\pi . f_{\mathrm{res}} \cdot \mu}{\sigma}} \\ k &= 2\pi . f_{\mathrm{res}} \cdot \frac{\sqrt{\varepsilon_r}}{c} \\ \eta &= \frac{377}{\sqrt{\varepsilon_r}} \\ Q_u &= \left(\frac{1}{Q_c} + \tan(\delta)\right)^{-1} \end{aligned} \tag{3}$$

Manuscript received June 25, 2001. This work was supported by the UofA NSF-S/IUCRC Center for Low Power Electronics under Grant EEC-9523338 and by the DigitalDNA Laboratories of the Semiconductor Products Sector, Motorola.

C. A. Tavernier is with the Department of Electrical and Computer Engineering, The University of Arizona, Tucson, AZ 85721 USA.

R. M. Henderson is with DigitalDNA Laboratories, Semiconductor Products Sector, Motorola, Tempe, AZ 85284 USA.

J. Papapolymerou is with the School of Electrical and Computer Engineering, Georgia Institute of Technology, Atlanta, GA 30332 USA.

Digital Object Identifier 10.1109/TMTT.2002.803428.

TABLE I
DESCRIPTION OF THEORETICAL PARAMETERS

Names	Descriptions
l, w, h,	Cavity length, width, and height
m, n, o	Eigenvalues. 1,0,1 for the fundamental mode
ε_r	Cavity filler relative Permittivity
c	Speed of light in the vacuum
η	Wave impedance in the filler
k	Wave number in the filler
σ	Cavity wall conductivity
R_m	Surface resistivity of the cavity walls
tan(δ)	Filler loss tangent
μ	Vacuum permeability
t	Feed wafer thickness
Q_e	External quality factor

$$Q_l = \left(\frac{1}{Q_u} + \frac{1}{Q_e}\right)^{-1} \tag{4}$$

where $f_{\rm res}$ is the resonant frequency, Q_c is the cavity quality factor, Q_u is the unloaded quality factor, and Q_l is the loaded quality factor. Table I describes the various parameters that appear in (1)–(4).

The quality factor (figure-of-merit) measures the ratio of power stored over power lost in the resonator and should be maximized. Three quality factors occur: Q_c only takes into account the loss in the cavity walls and Q_u adds the dielectric loss of the filler to the previous quantity. Finally, Q_l takes into account the losses added by the external excitation circuit. The previous values can be measured using the following set of equations [7]:

$$Q_l = \frac{f_{\rm res}}{\Delta f} \tag{5}$$

$$S_{21}\ (\text{dB}) = 20\log\left(\frac{Q_l}{Q_e}\right) \tag{6}$$

and

$$Q_u = \left(\frac{1}{Q_l} - \frac{1}{Q_e}\right)^{-1} \tag{7}$$

where S_{21} is the insertion loss, Δf is the bandwidth, and $f_{\rm res}$ is the resonant frequency. In order to increase the accuracy of the measured Q_u, the insertion loss should be greater than 9 dB.

The increase of the cavity height and wall conductivity directly increases the quality factor in (2). Therefore, highly conductive metals such as gold (used in this study) and silver with 4.1×10^7 and 6.1×10^7 S/m respective conductivity values are recommended. Increasing the filler height is limited by integration constraints and the dielectric loss of the filling material in (3). Beyond a certain loss tangent, it is not advantageous to increase the cavity height.

Another possibility for increasing the quality factor is allowed with the implementation of a square base $(l = w)$ (Fig. 1) and cubic cavity $(l = w = t)$ [12]. Fig. 1 shows the relationship between cavity size and quality factor. At 5.7 GHz and with a filler dielectric constant of 70, by varying the length in (1), the area of the cavity can be determined. In this case, the maximum Q is achieved when the length and width of the cavity are equal (square base). At low frequencies, e.g., 5 GHz, the permittivity of the filler will have to be very high in order to produce a cubic cavity with a reasonable size for silicon chip integration. Typically, with 2-mm side length, an ε_r of 450 is needed, as can be seen in Fig. 2, where the reported data neglect dielectric loss and the cavity walls are covered with gold.

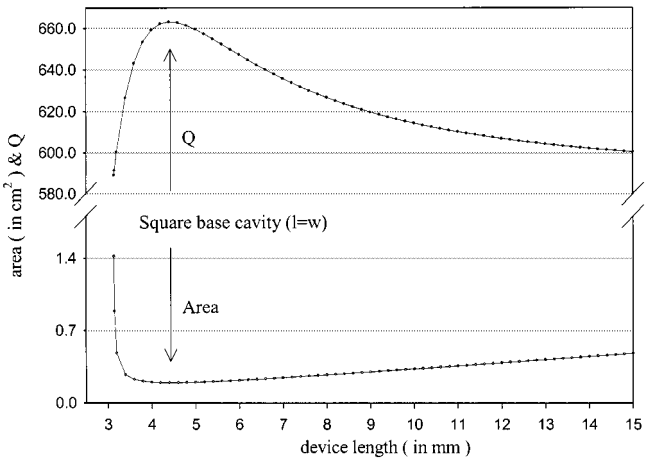

Fig. 1. Quality factor and cavity size for $\varepsilon_r = 70$ loaded cavity with $f_{\rm res} = 5.7$ GHz (1-mm thick: $\tan\delta = 0$).

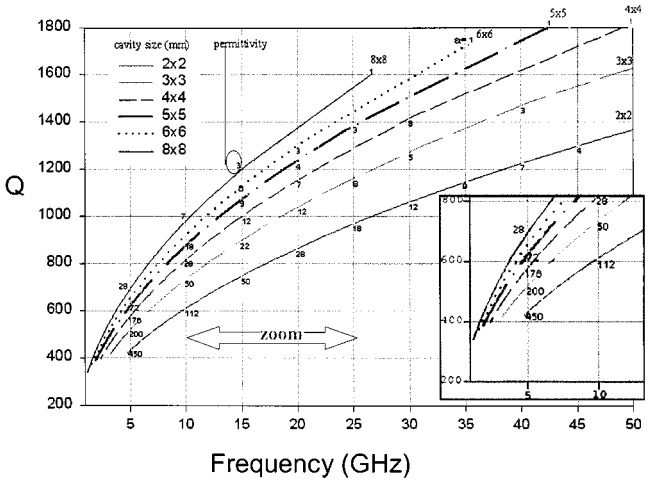

Fig. 2. Quality factor versus frequency for various fillers and square cavity (1-mm thick).

The tradeoff between performance and miniaturization is emphasized in Fig. 2. At a constant resonant frequency, an increase of the permittivity filler yields a reduced cavity size, but a lower quality factor as well.

III. RESONATOR OPERATION

The resonator is an assembly of a top and bottom wafer, with a loading material placed between the two wafers (Fig. 3). The top wafer, also called the feed, couples electromagnetic energy in the cavity, which is micromachined in the bottom wafer. As a result, the dominant cavity mode (TE_{101}) is excited. The magnetic coupling is ensured by two microstrip lines through two slots located in the ground plane of the top wafer. These two

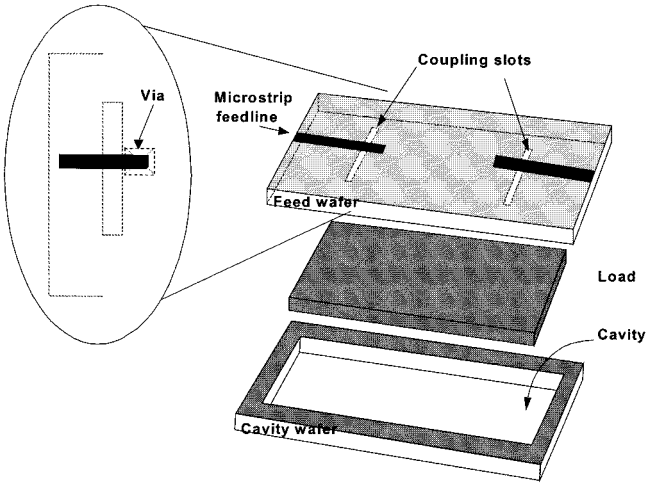

Fig. 3. Schematic of the micromachined cavity resonator filled with a dielectric material.

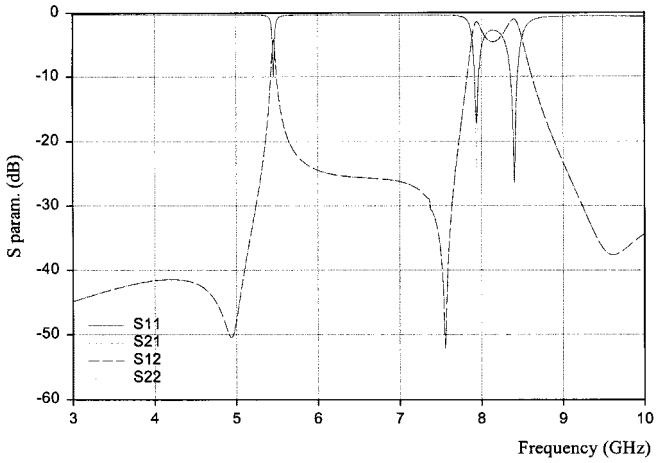

Fig. 4. Resonator simulated response with feed stubs.

apertures provide magnetic coupling by maximizing the magnetic field at their location. Bringing an electrical or a physical short next to the slot, between the ground plane and the microstrip line, maximizes the magnetic field by maximizing the current.

The physical short uses metallized vias, while the electrical short is a quarter-wavelength open stub, which reflects an open into a short. In the design of the last solution, fringing fields are taken into account and the physical length might be shorter than the quarter-wavelength. The bottom wafer, also called a cavity wafer, receives the high dielectric-constant loading material and is attached tightly to the feed wafer.

Fig. 3 represents the three separated elements. The cavity size and dielectric material inside determine the resonant frequency of the device, whereas the cavity height and dielectric loss impose restrictions on the quality factor [see (1)–(4)].

The resonator is simulated using Ansoft's High Frequency Structure Simulator (HFSS) 7.0. Once the geometry is drawn, boundaries are characterized. Ground and microstrip lines are modeled as a perfect electric conductor (PEC), whereas the slots are perfect magnetic conductors (PMC). Using the finite-element method, the geometry is discretized and meshed with tetrahedras near the resonant frequency.

In the design of the feed, particular attention should be given to the coupling slots. Their location affects the resonant frequency and rolloff. Positioning the slot a quarter cavity length away from each edge gives a satisfying result for rolloff, resonant frequency, and insertion loss [13].

Simulations for a BST cavity resonating at 5.7 GHz (Figs. 4–6), showed the superiority of vias over quarter-wavelength stubs in preventing the electric field from coupling between the two microstrip feedlines. Long stub lines produce substrate coupling effects (Fig. 5), which results in poor rolloff in the upper frequency band, as can be seen in Fig. 4. Vias provide the necessary shielding and minimize interactions between the two feedlines, as observed in Figs. 6 and 7. However, as it will be explained later there are fabrication limitations associated with vias in small-sized cavities.

In order to measure the micromachined resonators, it was necessary to include in the design a coplanar waveguide (CPW)-to-microstrip transition [14]. This transition included via-holes to ensure that the ground planes of the CPW sections were at the same potential with the microstrip ground. Table II summarizes the dimensions and electric parameters of the two micromachined cavity resonators that were designed.

IV. Fabrication

A high-resistivity 500-μm-thick silicon wafer (1–2-K$\Omega \cdot$ cm $\langle 100 \rangle$ orientation) was used for the fabrication of the feeding lines and the coupling slots in order to minimize loss. The wafer was covered with a layer of thermally grown oxide (0.8-μm thick). The oxide acts as a masking layer during the wet etching process. The microstrip lines were patterned using standard integrated circuit (IC) lithographic techniques, and were gold electroplated to a thickness of 3 μm. The bottom of the feed wafer that includes the coupling slots and vias was patterned using infrared alignment and metallized (Ti/Au) to a thickness of 1 μm with a liftoff process. After metallization, the oxide was removed only from the vias in order to proceed with the etching. The cavity wafer was a low-resistivity silicon wafer with a thickness of 1 mm. It was patterned with standard lithographic techniques to expose the area to be etched. Special marks for alignment purposes were also printed on it with a liftoff process.

After patterning, both wafers were immersed in a tetramethylammonium hydroxide (TMAH) water-based solution for silicon etching. A third wafer was attached to the cavity wafer with silver epoxy and then both wafers were metallized. The via-holes of the feed wafer were also filled with silver epoxy. In order to get optimum results, both the BST and the alumina dielectric materials were metallized (evaporation and Au plating), leaving two openings on the top surface to match the coupling slots in the feed wafer. By doing this, the conducting walls of the cavity are defined by the metal of the dielectric material, and air gaps between the different metal surfaces can be minimized. The etched cavity wafer acted as a package for proper alignment and bonding. Finally, after placing the metallized dielectric material inside the etched cavity wafer, the latter was bonded to

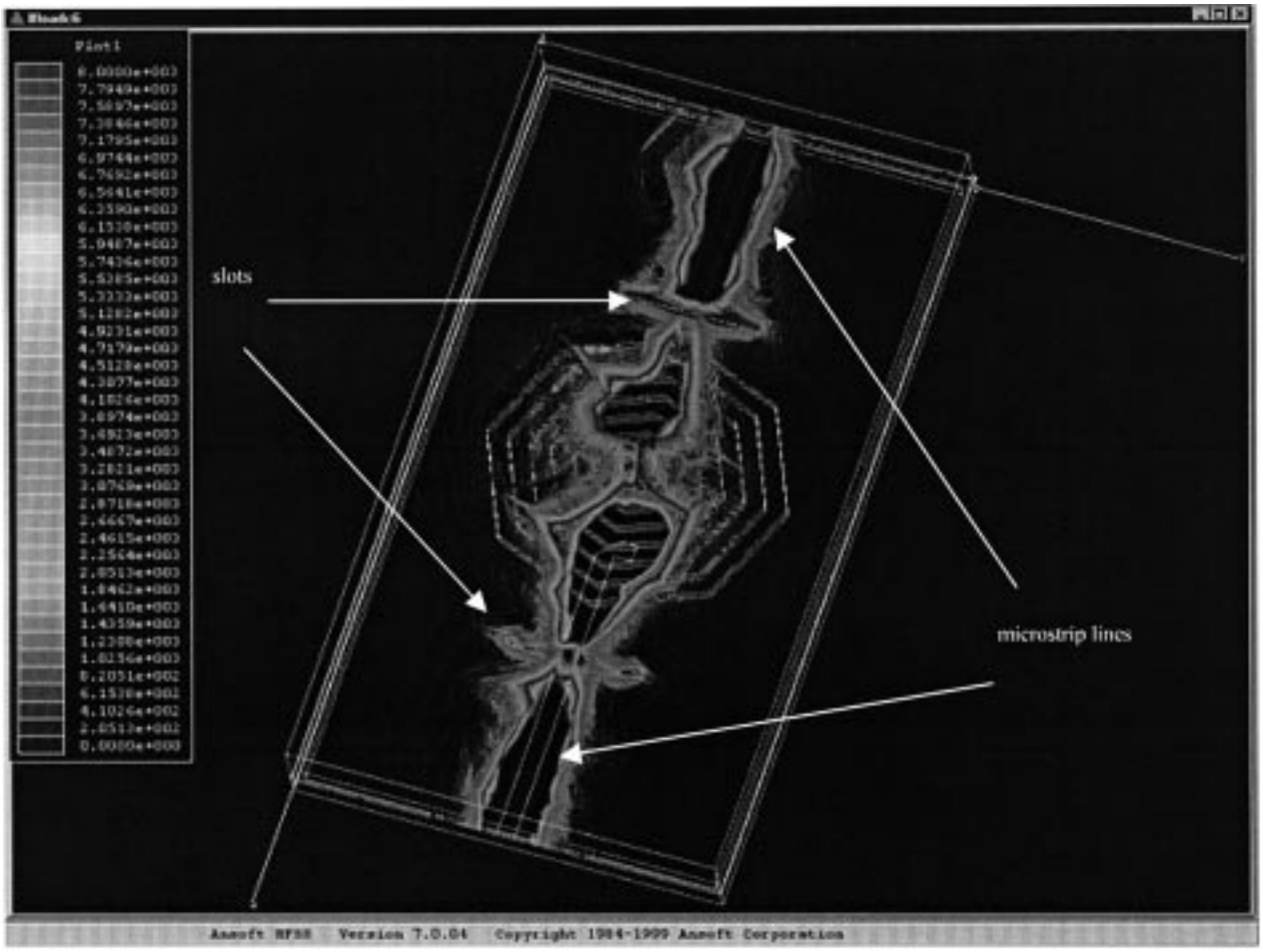

Fig. 5. Electric-field plot of top wafer for a resonator with open stubs.

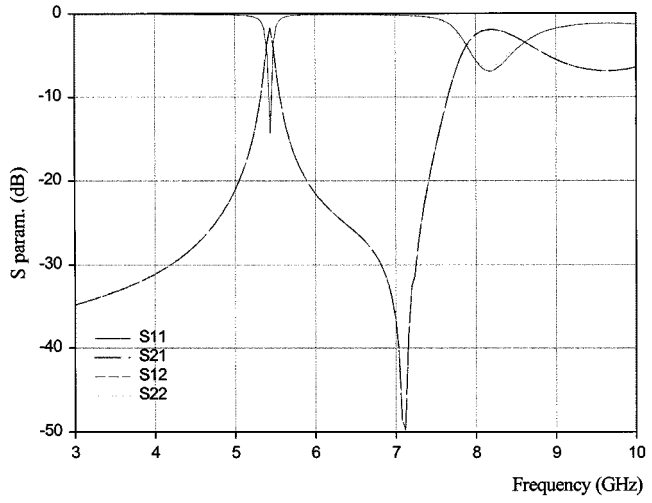

Fig. 6. Simulated response of the resonator with feed vias.

the feed wafer using an infrared bonding technique and silver epoxy. The silver epoxy was cured at 120 °C for 20 min.

During the fabrication, some limitations were discovered [15]. Despite (2) yielding a maximum for the square base cavity, which is also a minimum for the device area (Fig. 1), this configuration was not explored because of the implementation of wet-etched vias in the feed. This technique produces wide vias caused by the anisotropic etch along the $\langle 100 \rangle$ silicon crystal plane. Consequently, for a small cavity size and relatively thick feed, collision of the via-holes can occur and a cavity length to a width ratio of two is preferred. This was the case of the BST and alumina cavities. Along with the bonded resonators, some unbonded ones were also fabricated for testing purposes.

TABLE II
RESONATOR PROTOTYPE PARAMETERS

Parameters	Alumina resonator	BST resonator
l	18.47 mm	7 mm
w	9.58 mm	3.5 mm
h	1 mm	1 mm
ε_r	9.8	70
tan(δ) (filler)	0.0002	0.0024
σ (walls)	4.1×10^7 S/m	4.1×10^7 S/m
t	0.5 mm	0.5 mm
ρ (feed wafer)	1-2 KΩcm	1-2 KΩcm

V. RESULTS

A. Cavity Resonator With Alumina ($\varepsilon_r = 9.8$)

The feeding of the cavity was achieved using 50-Ω microstrip lines. The coupling slots were designed for optimum bandwidth

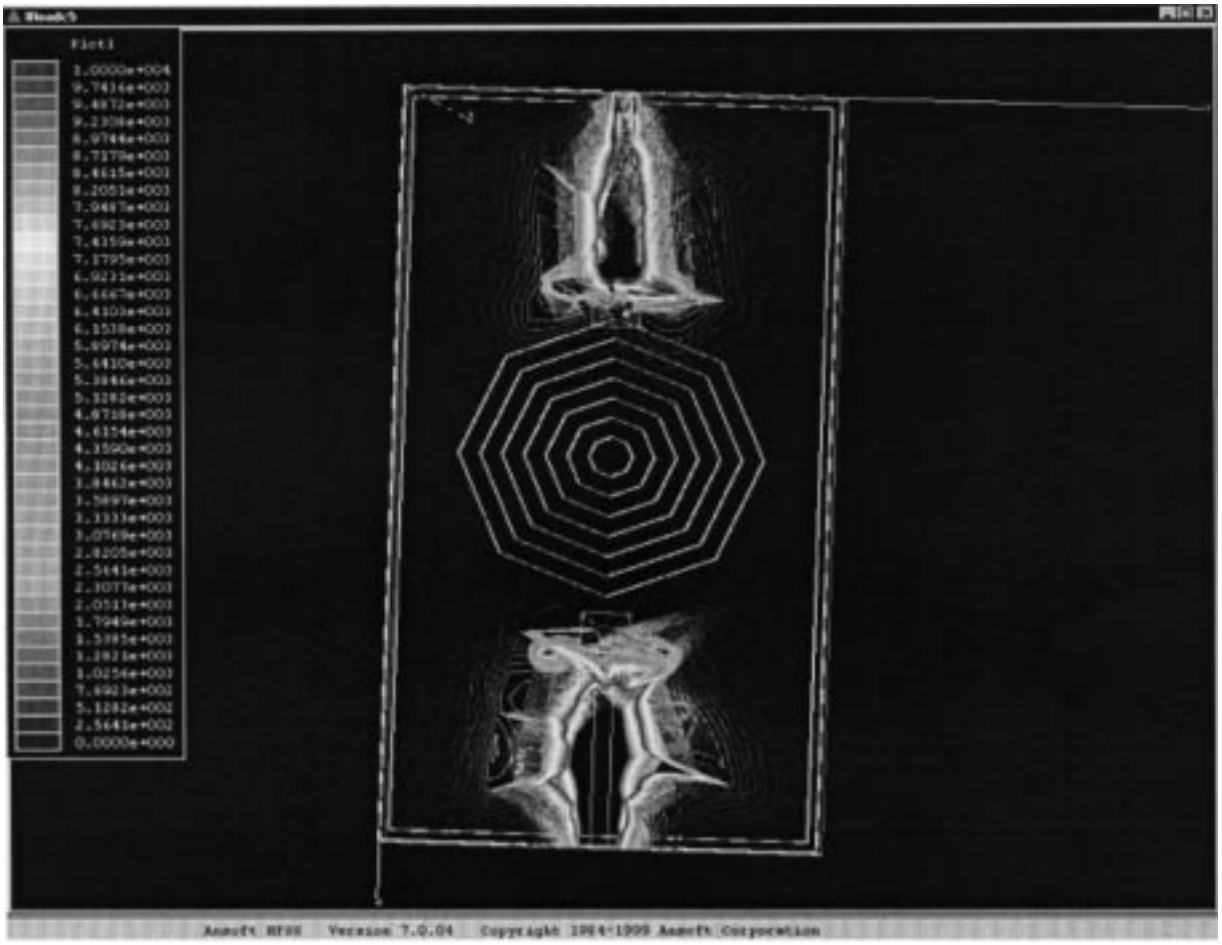

Fig. 7. Electric-field plot of top wafer for a resonator with feed vias.

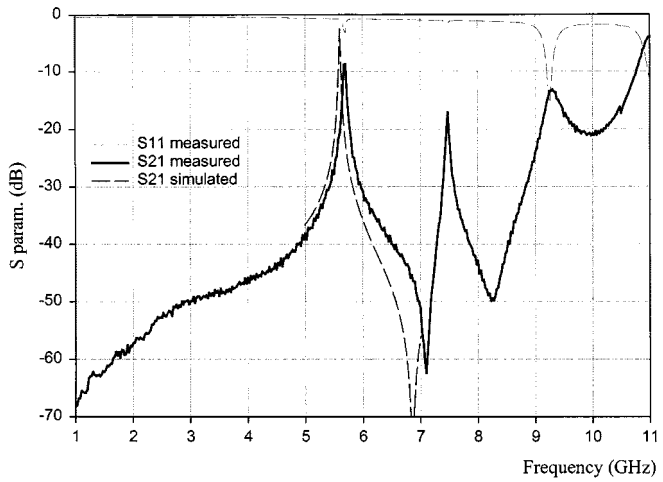

Fig. 8. Response for cavity resonator with alumina.

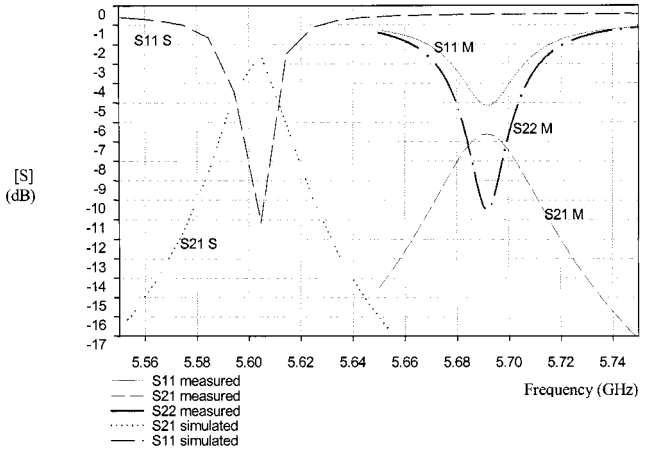

Fig. 9. Detail of the response shown in Fig. 8.

and insertion loss [optimal coupling (OC)]. In addition to the feedlines, the top wafer contained calibration standards in order to perform on-wafer thru-reflection-line (TRL) calibration. Using the standards, the reference plane was shifted to the center of the coupling slots. The resonator was measured on-wafer with an HP8510C vector network analyzer.

Prior to bonding, the resonator was measured in an unbonded configuration in order to estimate the response. In this case, pressure was applied by a dense metal screw sitting on the feed wafer far away from the microstrip lines. Etched windows corresponding to the patterned crosses in the cavity wafer were used for aligning the feed wafer.

Simulated and measured results of the bonded alumina resonator are shown in Figs. 8 and 9, respectively, for OC. The measured resonant frequency was 5.69 GHz, whereas simulation yielded 5.6 GHz for a permittivity of 9.8. This result is in

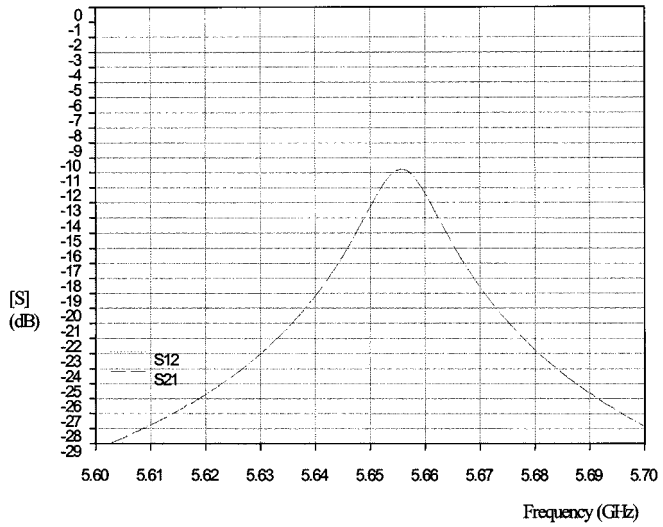

Fig. 10. WC response for the cavity resonator with alumina.

TABLE III
RESULTS FOR THE CAVITY RESONATOR WITH ALUMINA

Alumina cavity	f_{res} (GHz)	Δf (MHz)	S_{21} (dB)	Q_u
Equation	5.63	NA	NA	693
HFSS	5.6	19	-2.3	NA
Bonded meas. OC	5.69	36.5	-6.6	NA
Bonded meas. WC	5.656	12.5	-10.8	636
Unbonded meas. WC	5.656	10.5	-16	640

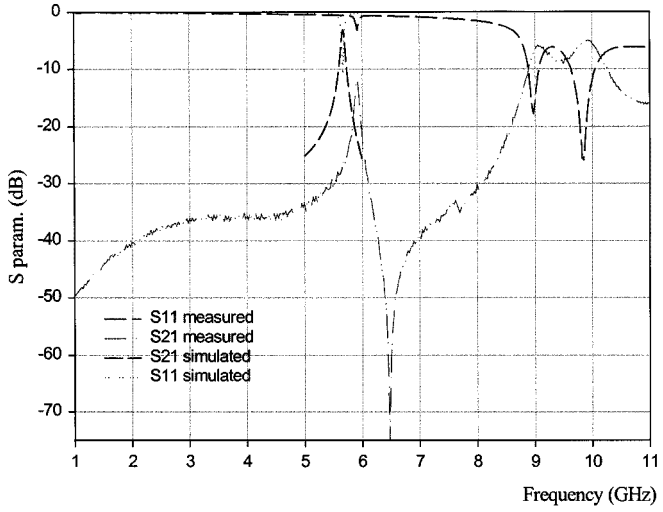

Fig. 11. Response of the bonded cavity resonator with BST.

good agreement with theory since the tolerance range given by the alumina manufacturer is $\varepsilon_r = 9.8 \pm 0.1$.

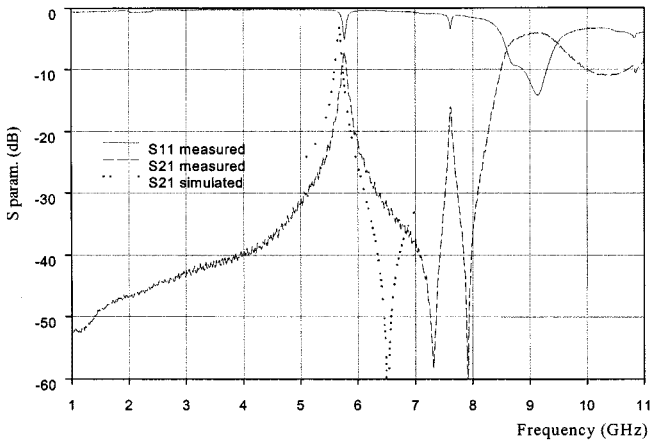

Fig. 12. Response of the unbonded cavity resonator with BST.

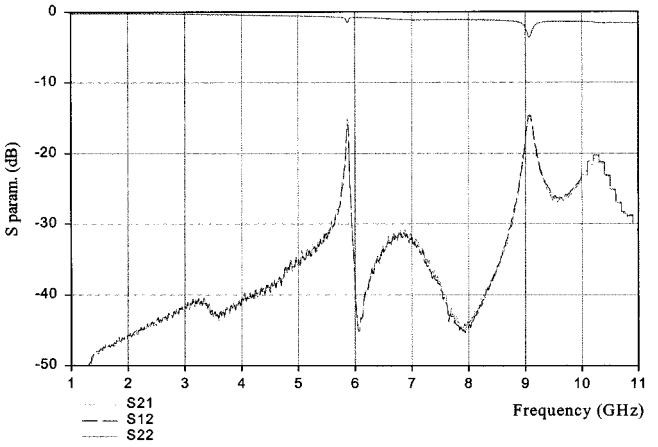

Fig. 13. WC response of the unbonded cavity resonator with BST.

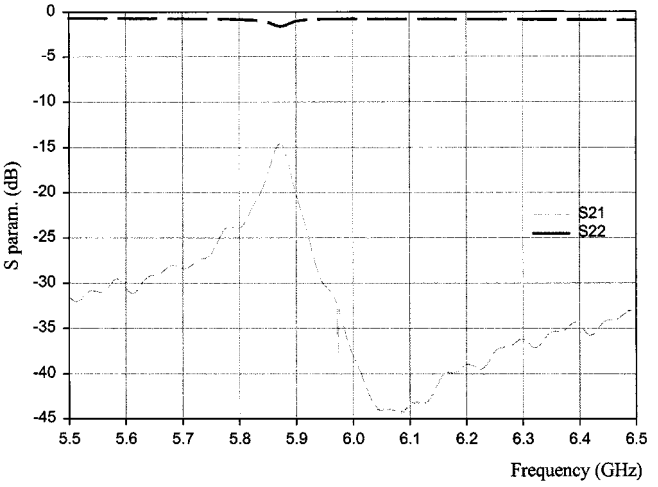

Fig. 14. Detail of the response shown in Fig. 13.

The bandwidth was measured to be 36.5 MHz and the insertion loss 6.6 dB. The increased loss can be explained by a misalignment between the slots of the top wafer and the slots of the dielectric filler, which produces mismatch and possible leakage. If properly enclosed and aligned, the cavity can yield

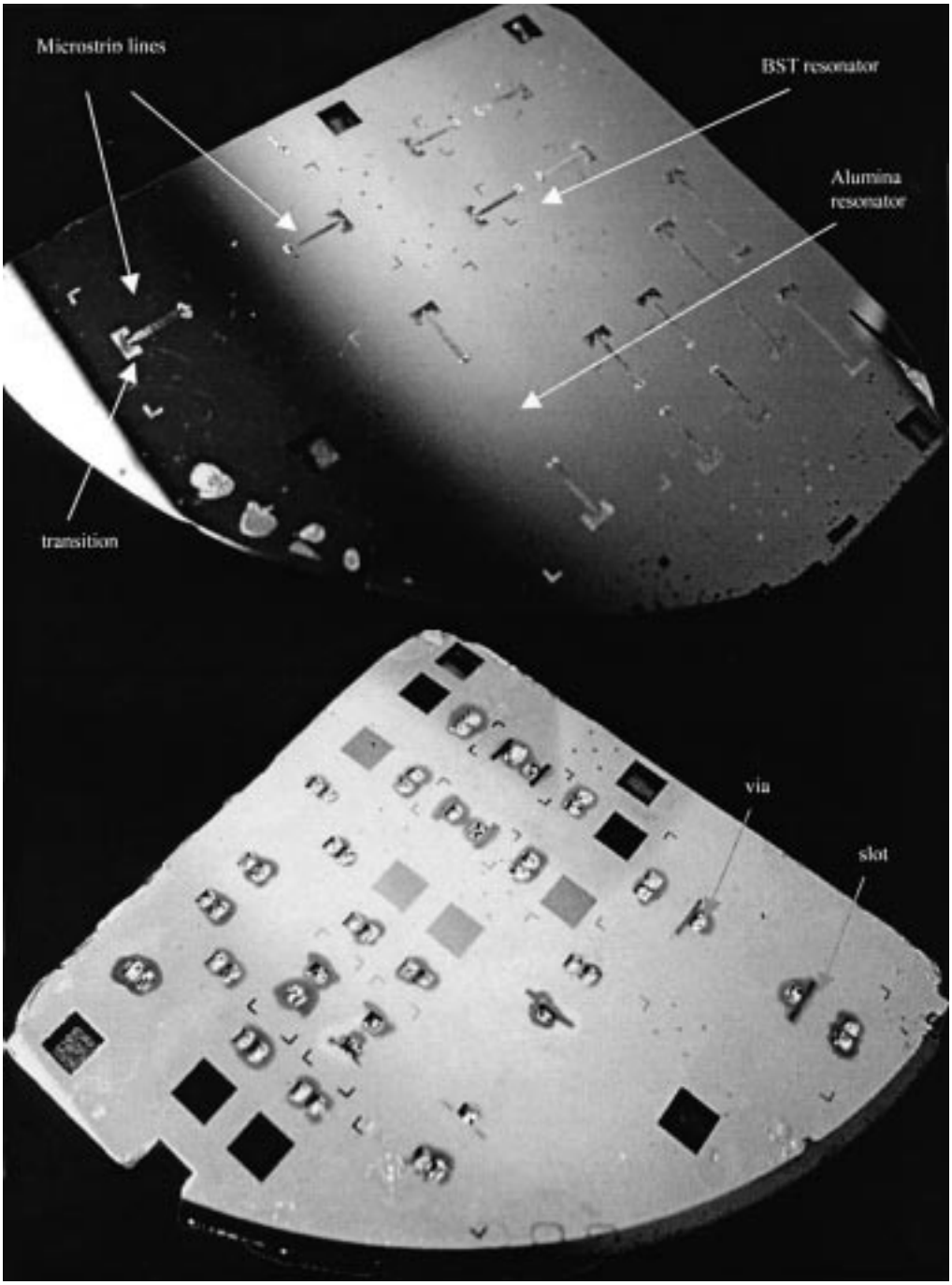

Fig. 15. Silicon top wafer (feedline and ground sides).

limited loss up to 0.8 dB [10]. In addition, since the reference point was located at the center of the slots, an evaluation of the loss generated by the via close to the slot (coupling via) is necessary for the experimental result to be accurate. The measurement of the response with the feed over a ground plane yielded 0.45 dB of loss per via. Consequently, the insertion loss would decrease if the via fabrication were improved. As seen in Fig. 9, the response presents an important asymmetry, which reflects the misalignment between the slots in the filler and feed. Cavity and feed wafer can be precisely aligned, but the lithography of the alumina slots and the cavity wet etching add significant inaccuracy when dealing with identical slot matching. Improvement of this issue is expected to significantly reduce the filter loss.

In order to accurately measure the quality factor, a top wafer with narrow coupling slots was fabricated to achieve a weak coupling (WC) of the resonator. Because of possible leakage and misalignment, the unbonded configuration yields high insertion loss, but also less accuracy. It still provides a first reading and is, therefore, proven useful.

Fig. 10 presents the measurement in the bonded configuration. The insertion loss was 10.8 dB and the bandwidth 12.5 MHz, which correspond to a loaded and an unloaded

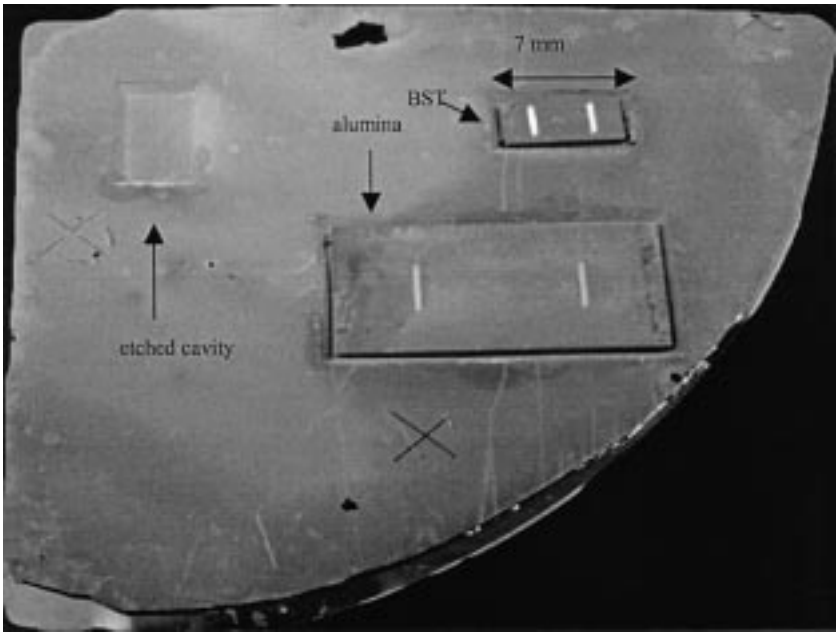

Fig. 16. Silicon cavity wafer with dielectric materials.

quality factor of 452 and 636, respectively, after applying (5)–(7). To the authors' knowledge, this is the highest value ever reported for this frequency and configuration. If one removes the loss from the coupling vias, Q_u is equal to 666. Despite higher coupling than expected, this result is in good agreement with theory ($Q_u = 693$), which does not take into account the presence of the slots.

Table III summarizes theoretical and experimental results and shows that the unbonded WC results were in agreement with the bonded measurements.

B. Cavity Resonator With BST ($\varepsilon_r = 70$)

A micromachined cavity filled with BST was also fabricated and tested. Due to the higher permittivity of the BST, the cavity dimensions were much smaller ($7 \times 3.5 \times 1$ mm^3) for a resonance around 5.7 GHz. The theoretical unloaded quality factor was 250 since the dielectric loss is higher than the one of alumina. During the fabrication, the Ti/Au seed layer used for the metallization of the dielectric was replaced by Cr/Au for a stronger adhesion on the BST polished surface. As in the previous section, an unbonded configuration was also explored for estimation of the response prior to the measurement of the bonded version.

Fig. 11 presents the comparison of the simulated and measured bonded BST resonator. The resonant frequency was measured to be 5.92 GHz, and the insertion loss was 10.9 dB for a 55-MHz bandwidth. The discrepancy in the resonator performance (higher loss) is explained by the limitation in manual alignment mentioned previously, which has a greater impact on a smaller geometry. The misalignment results in a strong mismatch and high loss.

In the unbonded configuration, better performance was obtained. Fig. 12 presents an OC measurement where the resonant frequency was 5.78 GHz, the insertion loss was 7.15 dB, and the bandwidth was 81 MHz. Moreover, to limit wafer manipulation, the calibration was simply a short–open–load–thru (SOLT), which left the reference planes at the probe tips. In order to deembed the microstrip-line loss up to the center of the slots, a thru line was measured. By removing this extra loss (1.8 dB), the actual resonator insertion loss was found to be 5.35 dB.

TABLE IV
RESULTS FOR THE CAVITY RESONATOR WITH BST

BST cavity	f_{res} (GHz)	Δf (MHz)	S_{21} (dB)	Q_u
Equation	5.73	NA	NA	252
HFSS	5.67	72	-3.2	NA
Bonded meas. OC	5.92	55	-10.9	NA
Unbonded meas. OC	5.78	81	-5.35	NA
Bonded meas. WC	5.915	45	-16.54	154
Unbonded meas. WC	5.87	38.75	-12.76	197

A WC measurement of the same piece in the unbonded configuration produced a quality factor of 186 at 5.87 GHz with the same calibration (Figs. 13 and 14). Removing the loss due to the line and the transition, a Q_u of 197 was achieved. Since narrower slots are used for the WC, the cavity is better enclosed by the metal and looks electrically smaller. Therefore, the resonant frequency is expected to shift higher. Finally, the measurement of the same BST piece was performed in the bonded WC configuration. The bandwidth was 45 MHz at 5.915 GHz with 16.5 dB of insertion loss and $Q_u = 154$. This lower Q compared to the unbonded case can be attributed to the manual alignment that becomes more critical for smaller geometries.

In comparison with the first BST cavity measurement (OC), the last measurement presents interesting similarities: high resonant frequency, high insertion loss, and relatively narrow bandwidth. Clearly, the slots in the feed and filler do not physically match, therefore, the cavity is well enclosed by the metal producing a higher resonance and a typical WC measurement. Better alignment techniques associated with strong bonding are expected to enhance these results and yield better performance than the unbonded case of Fig. 12.

Table IV summarizes the results achieved for BST. Measured and theoretical results agree well, taking into account the tolerance on the permittivity filler and the perturbation caused by the misalignment emphasized previously. Loss due to the shorting vias is not included (0.9 dB) and a $Q_u = 203$ can be achieved if the fabrication and assembly issues are minimized. Photographs of the fabricated resonators are shown in Figs. 15 and 16.

VI. Conclusions

Two silicon micromachined cavity resonators that operate between 5.6–5.8 GHz have been fabricated. The first resonator had a size of 18.47 mm $\times$ 9.58 mm $\times$ 1 mm with a dielectric load of $\varepsilon_r = 9.8$. It exhibited a loss of 6.6 dB and a bandwidth of 36.5 MHz (0.64%) at 5.69 GHz, while its unloaded quality factor was measured to be 640 at 5.66 GHz. The second resonator had a smaller size of 7 mm $\times$ 3.5 mm $\times$ 1 mm and an $\varepsilon_r = 70$. The best measured insertion loss was 5.35 dB with a bandwidth of 81 MHz (1.4%) at 5.78 GHz The unloaded quality factors ranged from 152 to 197 at 5.87 GHz.

Both of these examples show the potential of using loaded micromachined resonators for the fabrication of very small size, low-loss, and narrow-band planar filters and multiplexers at frequencies around 5.7 GHz. Clearly, the limiting factor for achieving higher Q values is the dielectric loss of the material filling the cavity. As new high ε_r dielectrics with lower loss are developed, higher Q values for smaller volumes will be possible. Accurate alignment combined with improved bonding techniques would also significantly decrease the insertion loss at the resonance. In addition, via fabrication with higher accuracy and higher conductivity metallization would enhance the performance as well. Even with these limitations, the resonators presented herein exhibit a relatively high Q for their small size, when compared with other planar structures. The resonator approach can, therefore, be competitive if the above fabrication issues are addressed.

An additional advantage of these resonators, apart from the minimum size, is the capability to include other devices or structures inside the cavity. These hosts can also be used to build frequency tunable devices such as electromagnetic bandgap resonators and filters.

References

[1] S. Lehtonen, V. Plessky, M. Honkanen, J. Koskela, J. Turunen, and M. Salomaa, "SAW impedance element filters toward 5 GHz," in *Proc. IEEE Ultrasonics Symp.*, 1998, pp. 369–372.

[2] G. Tsarenkov, "10+ GHz piezoelectric BAW resonators based on semiconductor multilayer heterostructures," in *Proc. IEEE Ultrasonics Symp.*, 1999, pp. 939–942.

[3] H. Meier, T. Baier, and G. Riha, "Miniaturization and advanced functionalities of SAW devices," *Trans. Microwave Theory Tech.*, vol. 49, pp. 743–748, Apr. 2001.

[4] L. Reindl *et al.*, "Design, fabrication, and application of precise SAW delay lines used in an FMCW radar system," *Trans. Microwave Theory Tech.*, vol. 49, pp. 787–794, Apr. 2001.

[5] S. Kobayashi and K. Saito, "A miniaturized ceramic bandpass filter for cordless phone systems," in *IEEE MTT-S Int. Microwave Symp. Dig.*, vol. 2, 1995, pp. 391–394.

[6] T. Arai, H. Ono, and K. Ayusawa, "Ba(Co, Nb)O3-based ceramics for super high frequency dielectric filter," in *Proc. 18th IEEE/CPMT Int. Electron. Manufacturing Technol. Symp.*, 1995, pp. 437–440.

[7] J. Papapolymerou, J. C. Cheng, J. East, and L. Katehi, "A micromachined high-Q X-band resonator," *IEEE Microwave Guided Wave Lett.*, vol. 7, pp. 168–170, June 1997.

[8] P. Blondy, A. R. Brown, D. Cros, and G. M. Rebeiz, "Low loss micromachined filters for millimeter-wave telecommunication systems," in *IEEE MTT-S Int. Microwave Symp. Dig.*, 1998, pp. 1181–1184.

[9] B. Guillon *et al.*, "Design and realization of high-Q millimeter-wave structures through micromachining techniques," in *IEEE MTT-S Int. Microwave Symp. Dig.*, 1999, pp. 1519–1522.

[10] C. A. Tavernier, R. Henderson, and J. Papapolymerou, "A hybrid micromachined high-Q cavity resonator at 5.8 GHz," in *Proc. 30th Eur. Microwave Conf.*, vol. 1, Paris, France, Oct. 2000, pp. 125–128.

[11] D. M. Pozar, *Microwave Engineering*, 2nd ed. New York: Wiley, 1998.

[12] R. F. Harrington, *Time–Harmonic Electromagnetic Field*. New York: McGraw-Hill, 1961.

[13] L. Harle, J. Papapolymerou, J. East, and L. P. B. Katehi, "The effect of slots positioning on the bandwidth of a micromachined resonator," in *28th Eur. Microwave Conf.*, Amsterdam, The Netherlands, Oct. 5–9, 1998, pp. 664–668.

[14] R. F. Drayton, "The development and characterization of self-packages using micromachining techniques for high frequency circuit applications," Ph.D. dissertation, The University of Michigan at Ann Arbor, Ann Arbor, MI, 1995.

[15] C. A. Tavernier, "Novel reduced-size micromachined resonators and filters," M.S. thesis, Dept. Elect. Comput. Eng., Univ. Arizona, Tucson, AZ, May 2001.

Christophe A. Tavernier received the DEUG degree in science pour l'Ingıieur from the University of Paris VI, Paris, France, in 1996, the Grandes Ecoles Engineering Diploma from EPF, Paris, France, in 1999, and the M.S. degree in electrical and computer engineering from the University of Arizona, Tucson, in 2001.

He is currently with the Electrical and Computer Engineering Department, University of Arizona. His main interest is the development of high-performance integrated passives at high frequencies.

Rashaunda M. Henderson (S'91–M'99) received the B.S.E.E. degree from Tuskegee University, Tuskegee, AL, in 1992, and the M.S. and Ph.D. degrees in electrical engineering from The University of Michigan at Ann Arbor, in 1994 and 1999, respectively.

In February 1999, she joined the Materials and Structures Laboratories (a division within Digital DNA Laboratories), Semiconductor Product Sector, Motorola, Tempe, AZ, where she is involved with characterization, simulation, and model development of on- and off-chip RF and microwave passive structures. Her research has involved developing and characterizing silicon-based packages fabricated with standard ICs and micromachining techniques for high-frequency applications.

Dr. Henderson is a member of the IEEE Microwave Theory and Techniques Society (IEEE MTT-S), the National Society of Black Engineers (NSBE), and Eta Kappa Nu. She is treasurer of the IEEE Waves and Devices Chapter Phoenix Section.

John Papapolymerou (S'90–M'99) received the B.S.E.E. degree from the National Technical University of Athens, Athens, Greece, in 1993, and the M.S.E.E. and Ph.D. degrees from The University of Michigan at Ann Arbor, in 1994 and 1999, respectively.

From 1999 to 2001, he was a faculty member with the Department of Electrical and Computer Engineering, University of Arizona, Tucson. In August 2001, he joined the School of Electrical and Computer Engineering, Georgia Institute of Technology, Atlanta, where he is currently an Assistant Professor. His research interests include the implementation of micromachining techniques and microelectromechanical system (MEMS) devices in microwave, millimeter-wave, and terahertz circuits, and the development of both passive and active planar circuits on Si and GaAs for high-frequency applications.

Dr. Papapolymerou was the recipient of the 2002 National Science Foundation (NSF) CAREER Award and the 1997 Outstanding Graduate Student Instructional Assistant Award presented by the American Society for Engineering Education (ASEE), The University of Michigan Chapter.